
# Journal Paper

"Condition Monitoring System for Solar Power Plants with Radiometric and Thermographic Sensors Embedded in Unmanned Aerial Vehicles"

- Measurement -

March 2019

Fausto Pedro García Márquez

Ingenium Research Group, Universidad de Castilla-La Mancha

FaustoPedro.Garcia@uclm.es

Isaac Segovia Ramírez

Ingenium Research Group, Universidad de Castilla-La Mancha

Isaac.Segovia@uclm.es

Cite as: Márquez, F. P. G. & Segovia, I. (2019). Condition Monitoring System for Solar Power Plants with Radiometric and Thermographic Sensors Embedded in Unmanned Aerial Vehicles. Measurement

DOI: https://doi.org/10.1016/j.measurement.2019.02.045

# Condition Monitoring System for Solar Power Plants with Radiometric and Thermographic Sensors Embedded in Unmanned Aerial Vehicles

Fausto Pedro García Márquez, Isaac Segovia

Ingenium Research Group, Universidad Castilla-La Mancha, 13071 Ciudad Real, Spain.

[isaac.segovia; faustopedro.garcia@uclm.es

**Abstract**

The photovoltaic solar energy industry is expanding, and there is therefore a need to increase and improve its maintainability, operating costs, availability, reliability, safety, life cycle, etc. The aim of this article is to design, develop and check a new condition monitoring system to detect dust in solar photovoltaic panels. The condition monitoring system uses a radiometric sensor connected to an Arduino platform. This novel approach is based on emissivity analysis produced over a surface and characterized with a low emissivity value when dust appears. A thermographic camera is also employed to validate the results provided by the radiometric sensor. The system is designed to be embedded in an unmanned aerial vehicle. Radiometric data is sent and analysed, Internet of Things is employed, and thermograms are stored for further processing. Several scenarios with a real solar panel are used in the experiments, in which the angles and distances of the sensors and surface conditions are studied. An analysis of the radiometric sensor provides accuracy results, and the presence of dust is identified in all scenarios.

**Key Words:** Radiometric Sensor, Infrared Thermography, Solar Photovoltaic Energy, Condition Monitoring System, Remotely Piloted Aircraft, Non-Destructive Testing.

# 1 Introduction

The use of renewable energies is rising and there is greater world energy demand [1]. They are based on endless resources, e.g. the sun, wind, or any resource with sustainability. One of the most significant types of renewable energy is solar energy which involves the use of photovoltaic (PV) panels, and which are in continuous development and expansion [2]. The most significant growth of solar energy has been seen in Asia, mainly in China and Japan, with 15.2 and 11 GW respectively, followed by the United States [3]. The European market is also rising, mainly in United Kingdom, Germany and France [4].

PV farms are usually located in areas with certain climatic conditions, e.g. high solar radiation. Costs, maintenance tasks and downtimes need to be reduced, and productivity increased in order to achieve competitiveness in the energy market [5,6].

Supervisory Control and Data Acquisition (SCADA) is employed in most companies that manage maintenance polices [7]. Advance analytics is employed to process the dataset [6,8], e.g. in fault detection and diagnosis [9,10]. SCADA monitors, for example, electrical variables of the PV power generation system [11], but it does not monitor the PV panel surface. New condition monitoring systems (CMS) are used to inspect superficial defects of the PV panels [12].

Fault detection algorithms are employed to monitor the condition of PV panels [13]: pattern recognition based in electric output is considered in reference [14]. Combined artificial neural network and analytical based methods are employed for automatic fault detection and diagnosis for PV systems by Jiang, and Maskell (2015) [15], where Karatepe and Hiyama (2011) [16] employed neural networks, etc. Jaffery et al. (2017) [17] used Fuzzy logic systems to predict failures. Spataru et al. (2013) [18] utilized pattern recognition by temperature and irradiance to show power output and predict power losses in the short term. Zorrilla-Casanova et al. (2011) [19] employed signal processing in temperature, humidity, power output and wind speed signals. Aix-layer detection algorithm is used by Dhimish et al. (2017) [20] to detect failures and study the power output of the modules. Finally, statistical approaches can be found in references [21,22].

Traditional maintenance polices, e.g. visual inspection, are unviable in terms of cost and operating time. Therefore, it is necessary to design and develop new monitoring systems [23,24]. Defects in solar panels show patterns that directly affect surface

temperature [25]. It is an important parameter that must be measured to detect and identify the main failures, for example: hot spots browning; snail trails: cracked cells; burned; cell or module broken; broken interconnects; solder bond failures; dirty points, etc. [26]. Faults need to be detected as early as possible to ensure the performance and reliability of PV systems [23].

New CMSs embedded in an unmanned aerial vehicle (UAV), employing thermographic sensors, are now used in maintenance tasks [27]. This system is a non-destructive testing (NDT) that is able to perform measurements without interfering in the integrity of systems [28-30]. These techniques are carried out in the predictive maintenance of different industrial areas, reducing costs associated with manual inspections and maintenance periods [31,32]. Infrared thermography is now one of the most NDT techniques used in UAVs [33,34].

Thermography allows the visualization of the surface temperature by capturing variations of infrared radiation. The radiated energy, measured by a thermographic camera, is converted into temperature values with detectors or thermal sensors that compare measured radiation with fixed values, depending on the camera, that assign color palettes to each temperature value [35]. Currently, this technique is used due to its technical advantages [36].

Thermography in PV panels has been studied in detail in laboratories [37], in which cracked silicon wafers, hot spots, etc have been analyzed. [38,39]. However, PV thermography inspection presents difficulties in data processing and interpretation. Advanced algorithms are required to analyse thermograms to detect panels and identify faults [40].

UAVs are vehicles powered by one or more engines, capable of maintaining a controlled and self-sustaining flight level [26]. These systems are built with stabilization systems to transport different sensors. UAVs have multiple advantages, e.g. speed, safety, costs and a large angle of vision [41]. UAVs have been adapted for different applications due to their high technical conditions. They are mainly used for photography, thermography, safety and rescue. They are also used in renewable energies, specifically to analyze blades of wind turbines and PV panels [42,43]. The combination of drones and infrared thermography allows maintenance tasks to be optimized [23], achieving significant economic and operational advantages [44]. The main advantages of aerial

thermography/radiometry using drones are: the ability to reach difficult access areas to obtain real data, reduce operational risks, increase operator safety, and reduce data collection time. It demonstrates greater reliability compared to conventional methods and is cost saving, at a rate of approximately 40% compared to conventional methods [45].

Dirt, dust, ice or other elements deposited on the panel, as well as shadows and adverse weather conditions, cause a loss of energy production [46]. Dirt on the PV panels and changes to the incidence solar radiation angle might cause a significant loss in annual energy production of 5%, that can reach 15% in periods without rain - see Figure 1. The study was carried out in four monocrystalline silicon modules with three different types of glass, using flat and texture glass [47].

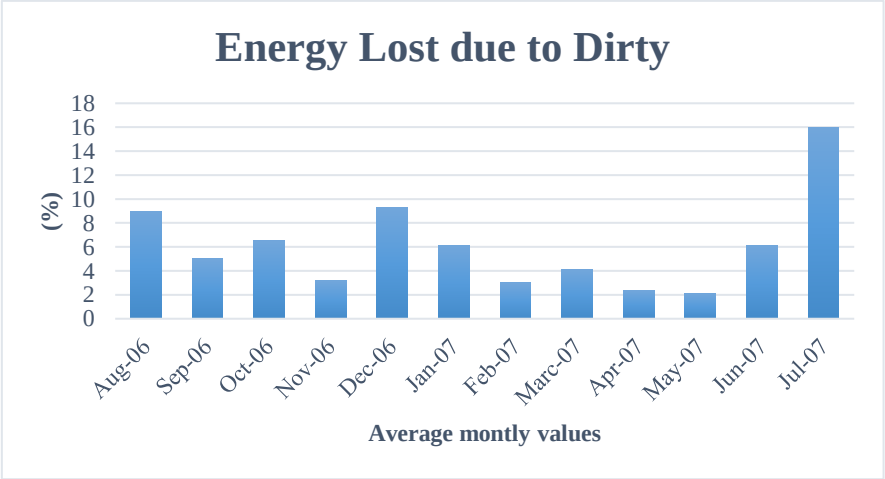


Figure 1: Estimated monthly average values for dirt losses [47]

García et al. (2011) [48] analyzed the soiling and the angle of incidence (AOI) to measure optical losses in a vertical-axis tracked solar plant in Spain. They concluded that optical losses vary from 1 to 8% in tracking surfaces, and 8 to 22% in horizontal ones, with greater percentages in dry periods. Kimber et al. (2006) [49] studied the soiling in rural, suburban and urban scenarios in EEUU. The results showed that the soiling rate is greater in the desert, and the correlation between rain and efficiency of the modules is higher. Aron and Littmann (2013) [50] considered the energy lost due to soiling, compared the voltage of two modules, one of which was periodically cleaned, and concluded that the soiling rate varies from 1 to 11.5%, indicating that it greatly depends on the environment. Similar research studies can be found in [51-54]. Acciani *et al.*

proposed a generic analysis of PVs that use thermography, concluding that dirt can be identified as dark regions in thermal images [55].

A large number of studies have been conducted in order to mitigate the dirt on the PV panels. In a Malaysian case study, Jamil et al. (2017) [56] presented a review of mitigation methods that perform degradation of photovoltaic power systems. In EEUU, Mazumder et al. (2015) [57] showed the environmental degradation of the optical surface of PV modules and solar mirrors by soiling and high RH and mitigation methods for minimizing energy yield losses. Moharram et al. (2013) [58] studied the influence of cleaning by using water and surfactants on the performance of photovoltaic panels in Egypt. Aly et al. (2015) [59] analyzed a novel dry cleaning machine for photovoltaic and solar panels in Saudi Arabia and Qatar, where similar work in Italy was undertaken by Tucci et al. (2002) [60]. Li et al. (2016) demonstrated a fast and robust mapping with low-cost Kinect V2 for a photovoltaic panel cleaning robot. The study was carried out in China and Italy. Alshehri et al. (2015) undertook a review of dust mitigation in the desert that involved the cleaning mechanisms of solar panels in arid regions. Finally, Jones et al. (2016) described the optimized cleaning cost and schedule based on observed soiling conditions for photovoltaic plants in central Saudi Arabia.

The PV field could not receive a uniform irradiation in panels or single cells, working at the same temperature. Therefore, mismatches among different parts of the array may arise. This effect has been studied in literature, e.g. [61,62]. Petrone et al. (2007) [63] proposed a model based in Lambert W-function that is able to describe the behavior of matched as well as mismatched PV fields. Chouder and Silvestre (2009) [64] considered a novel procedure to study the power losses mainly due to mismatch effects, extracting the main PV module and PV array parameters from I-V characteristics. The method allows a good estimation of the mismatch effect on the total PV system power losses.

This paper proposes a new CMS using a radiometer sensor and embedded in an UAV according to Figure 2, to detect dust on PV panels.

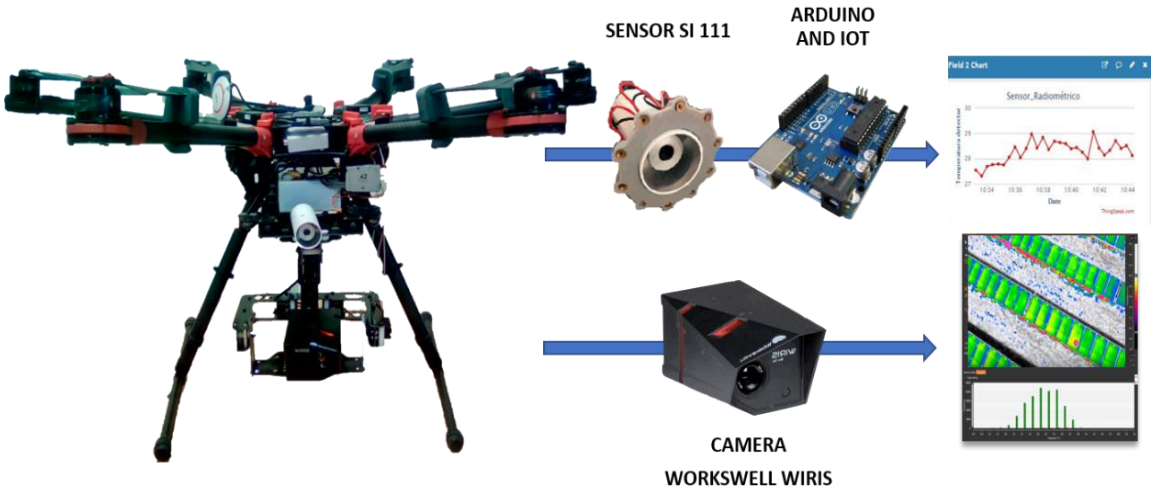


Figure 2: CMS diagram

Radiometry is employed to obtain the measurement of electromagnetic radiation. Invisible radiation to the human eye is measured quantitatively using sensors and/or detectors that convert part of the radiation into electrical signals [65]. These sensors capture the infrared energy emitted by objects through a detector, and it is transformed into an electrical signal to obtain the temperature value using a thermocouple or photodiode [66]. These devices present important advantages in comparison with thermographic cameras, e.g., lower cost, reduced weight and form, easy to transport and fast data processing, etc. [67]. The measurements are more reliable when environmental conditions (humidity and air temperature, distance to the object, reflected temperature, incident radiation, etc.) and surface characteristics, e.g. emissivity, are known [68]. In addition, it is necessary to consider the field of view (FOV) of the sensor (Figure 3), the perpendicular distance to the target or surface to be measured, and the angle of the sensor with respect to the vertical, due to its influence on the shape and area of the target surface. Figure 3 shows the influence of orientation in FOV. FOV depends of the angle of measurement, where values greater than 20º will produce extended ellipse.

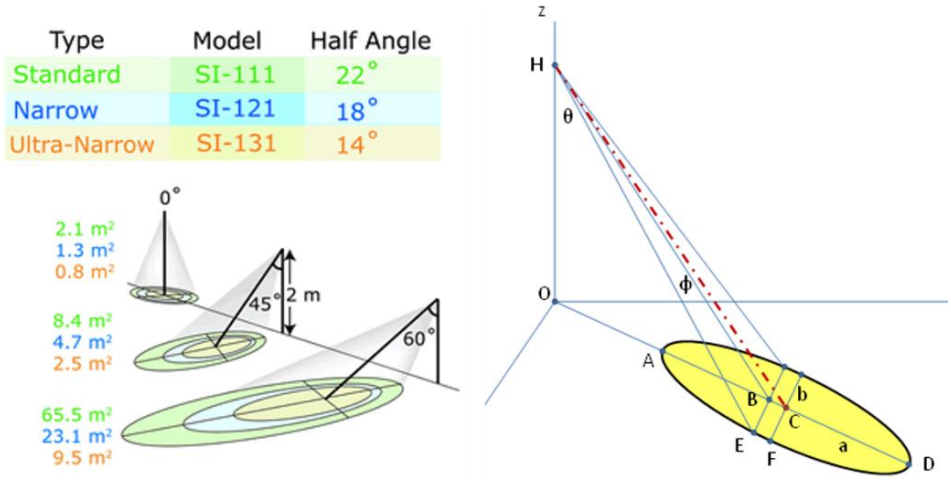


Figure 3: Variation of the target area as a function of FOV, altitude and angle [69]

The main contribution of this paper is to design, develop and test a new CMS to detect dust in PV panels. The CMS is embedded in a UAV. The CMS employs a radiometric sensor, and the results are validated by a thermographic camera. The approach is based on the emissivity that is produced over a surface, characterized with a low emissivity value when dust appears. Several scenarios were conducted using real solar PV panels.

## 2 Materials and Methods

The CMS proposed in this paper is based on a radiometric sensor and a data acquisition wireless system embedded in a UAV (Figure 4). The sensor measures the infrared signal, and an Arduino board transforms it into a suitable thermal value by electronic circuits. Arduino sends it to a wireless platform where the data is analyzed. The DJI S900 UAV is employed in this paper.

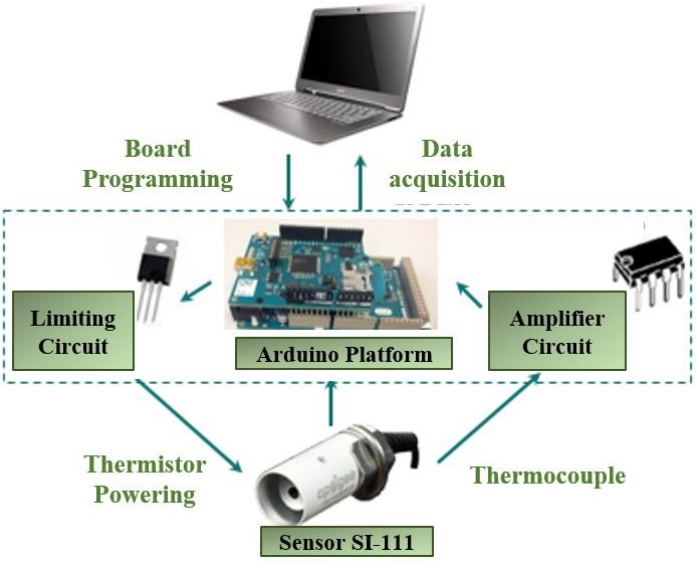


Figure 4: Infrared acquisition system diagram.

The radiometer sensor type is a SI-111 model with a germanium lens. The specifications of the sensor are detailed in Table 1.

Table 1: Technical characteristics.

| | | | |
|---|---|---|---|
| **Input Power** | 2.5 V excitation for thermistor | **Target Output Signal:** | 60 µV per ºC difference from sensor body |
| **Absolute Accuracy** | ±0.2 ºC; -10 to 65ºC<br>±0.5 ºC; -40 to 70ºC | **Body Temperature Output Signal** | 0 to 2500 mV |
| **Uniformity:** | ±0.1 ºC; -10 to 65ºC<br>±0.3 ºC; -40 to 70ºC | **Optics** | Germanium lens |
| **Repeatability:** | ±0.05 ºC; -10 to 65ºC<br>±0.1 ºC; -40 to 70ºC | **Wavelength Range** | 8 to 14 µm |
| **Response Time:** | Less than 1 second to changes | **Field of View** | 22º half angle |
| **Operating Environment:** | Highly water resistant, designed for continuous outdoor use. Operating range is -55 to 80ºC, 0 to 100% RH | | |

The sensor is connected to an Arduino DUE board with 32-bits. The Arduino provides the power to the sensor, collects the signal of the sensor, transforms it to temperature measurement by the Wi-Fi Shield module, and it is then sent to an online platform. The Arduino needs specific limiting and amplifier circuits for the signals, indicated in Figure 5. The sensor excitation power supply must be equal to or greater than 2.5V. The

LM137 monolithic regulator is used to adapt the 5V power supply of the Arduino to the required voltage. The sensor model has a thermal sensitivity of 20 µV per ºC. However, the Arduino DUE has a maximum of 12 bits, and the maximum voltage of its analogue inputs and outputs is 3.3V, therefore, its resolution is 40 times higher. The thermopile output differential signal is amplified with a voltage amplifier circuit to be read by Arduino. The analogue device AD-620 type is used.

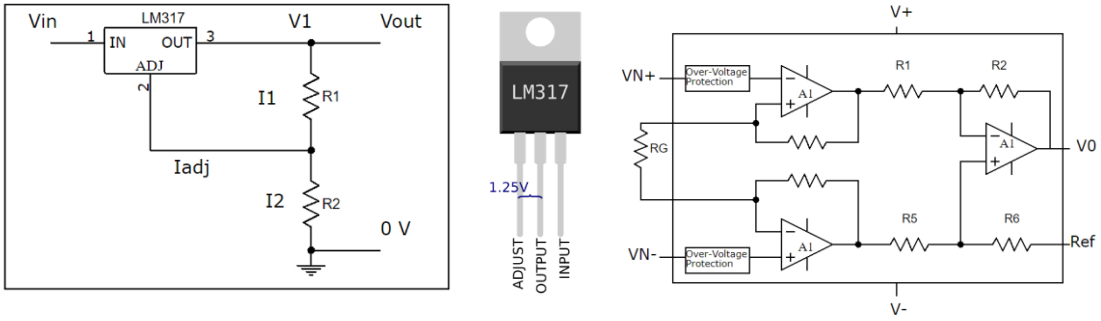


a b

Figure 5: and Amplifier circuit (a) and Voltage limiter circuit (b).

A thermography camera Workswell WIRIS type is used to validate the results. The camera is a thermal imaging system developed for use in UAVs. This model is light weight and it is equipped with an infrared (thermographic) camera and a visible spectrum camera. The analysis of thermograms is carried out by Corel Player software [44].

The PV panel used is TSM-170D, by the manufacturer Trina Solar (Figure 6). It is used in the industry, and it has been analyzed and compared with other models in reference [70].

Figure 6: PV panels used in the tests.

Table 2 shows the main parameters of the TSM-170D PV panel.

Table 2: Technical characteristics of the TSM-170D module.

| Parameters | TSM-170D |
|---|---|
| **Maximum Power** | 170 W |
| **Voltage in Open Circuit** | 43.60 V |
| **Short Circuit Current** | 5.25 A |
| **Voltage in Maximum Power** | 35.8 V |
| **Current in Maximum Power** | 4.76 A |
| **Maximum Voltage of the System** | 700 V |
| **Range of temperatures** | -40ºC, +90 ºC |
| **Dimension of the module** | 1581x809x40 mm |
| **Cell Type** | Monocrystalline |
| **Number of cells/ Cell Dimension** | 72 cells/ 125x125 mm |

ThingSpeak platform is employed to record and analyse the signal from the radiometric sensor. It is an Internet of Things (IoT) platform that provides an application programming interface to collect, store and visualize all the data obtained from a sensor online. Its operation is based on channels. Figure 7 shows the interface of this platform.

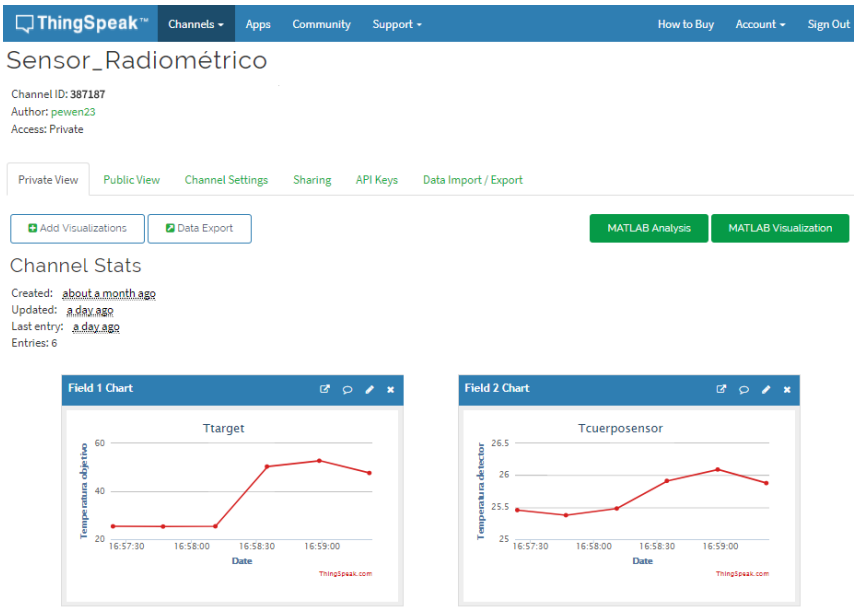


Figure 7: ThingSpeak interface.

# 3 Case Study and experiments

Three scenarios with different distances and angles have been set up to determine the accuracy and effectiveness of the sensor in different case studies. Finally, two scenarios are studied to analyze the influence of calibration and angles, where the CMS is embedded in a UAV.

The PV module used converts 6-20% of solar radiation into electrical energy, depending on the environment conditions: the influence of humidity on PV performance is directly related to the irradiation flux due to water droplets, a change in direction of solar radiation, and if the exposition is for a long time, humidity causes delamination [71]. The wind velocity produces a cooling in the cell temperature, obtaining a better efficiency [72]. The most important condition is the operation temperature, where several studies show predictive models and analyse the correlations with the temperature of the PV module [73-75]. Skoplaki and Palyvos conclude that the operating temperature is a key factor to understand the behavior of the PV panel [76]. Therefore, the environment conditions have been controlled in the experiments to minimize their influence on the measurements.

The results from the radiometer sensor are validated with the thermal images. The radiometer sensor provides the temperature of the sensor body and the target temperature,

i.e. the temperature of the measured surface. The variables that determine the shape and area measured by the sensor are the FOV, the sensor angle ($\phi$), the height ($h$) to the panel and the measurement angle ($\theta$), defined as the angle formed by the sensor with the perpendicular to the surface to be measured (Figure 3). The data collected from the sensor and camera are synchronized. The data not synchronized is discarded in order to avoid incorrect measurements. Figure 8(c) shows the LED marker system adapted to the sensor. It is used so that the FOV can be seen online. Figure 8(a) shows the CMS in the DJI S900 UAV with the panel and the LED marker system Figure 8(c). Figure 8(b) shows the Arduino board and electronic circuits.

A

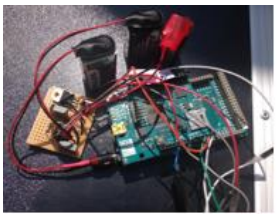

b

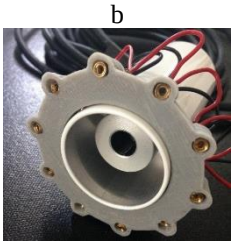

c

Figure 8: PV panel, DJI S900 and CMS (a), Arduino and electronic system (b) and the laser marker (c)

The sensor has been used without calibration because the main objective is to analyse patterns rather than real temperatures. The results are also validated using the sensor calibrated. 10 synchronized measurements of the sensor and the thermographic camera are taken. 3 and 4 areas, called *Zi*, of the PV panel are studied regarding to the following scenarios

Case study 1 considers 3 scenarios. Figure 9 shows each diagram of the scenarios and pictures:

- **Scenario 1.1:** It is set by the panel in horizontal position, supported on the ground, where $\theta = 0^{o}$, Figure 9(b). In Z3 small surface of dust is induced, where Z1 and Z2 are free of dust.
- **Scenario 1.2**: The panel is 70º regarding the vertical, where $\theta = 10^{o}$, see Figure 9(d). In Z3 a small film of dust is induced. Z1 and Z2 are free of dust.

- **Scenario 1.3:** It analyzes the dirt over the panel by depositing sand in a third of the area marked as yellow in Figure 9(e), the panel is 10º regarding the vertical and $\theta = 10^{o}$. This scenario considers 4 zones instead of 3. Z1 is free of dust, similar to Z1 in scenarios 1.1 and 1.2. Z2 indicates dust in one border, Z2 has 75% free of dust and 25% with dust, and Z3 is full of dust.

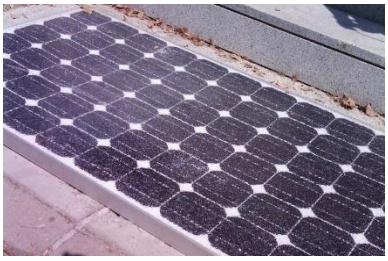

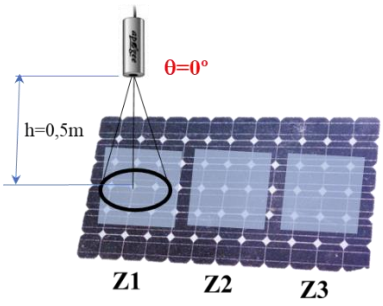


a b

Scenario 1.1

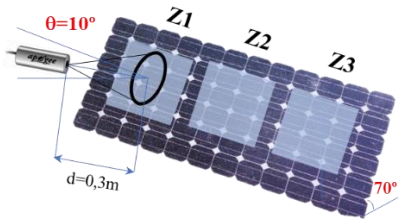


c d

Scenario 1.2

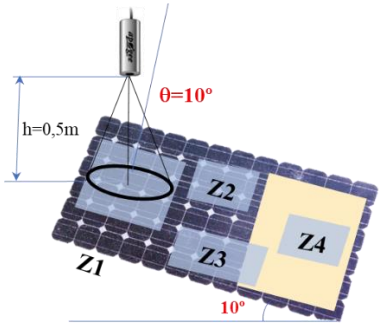


e f

Scenario 1.3

Figure 9: Case study 1 formed by 3 different scenarios. Diagram (top) and real equipment (bottom).

Case study 2 shows the sensor calibrated and not calibrated, both embedded in the UAV. Two scenarios are analysed:

- **Scenario 2.1**: The PV panel is in a horizontal position, supported on the ground, where $\theta = 0^{o}$. The panel is partially covered with dust.

- **Scenario 2.2:** The PV panel is in panel in a horizontal position, supported on the ground, where $\theta = 60^{o}$. The room temperature is lower than in case study 1.

# 4 Results

The measurements were recorded at the same time and weather conditions for case study 1, with sunny days. Figure 10 shows the experiments for Scenario 1.1, where the three zones Zi in Figure 9 are analyzed. Table 3 shows the temperatures given by the radiometer sensor in Z1, Z2 and Z3. The panel is set in a horizontal position and $\theta = 0^{o}$. The temperature given by the radiometer sensor are different regarding Zi, the maximum difference being in Z3, where the dust is. The results are validated by the thermography analysis shown in Figure 10. The temperatures in Z1 and Z2 are almost the same, see Table 3, and the difference is mainly due to the area that is analyzed.

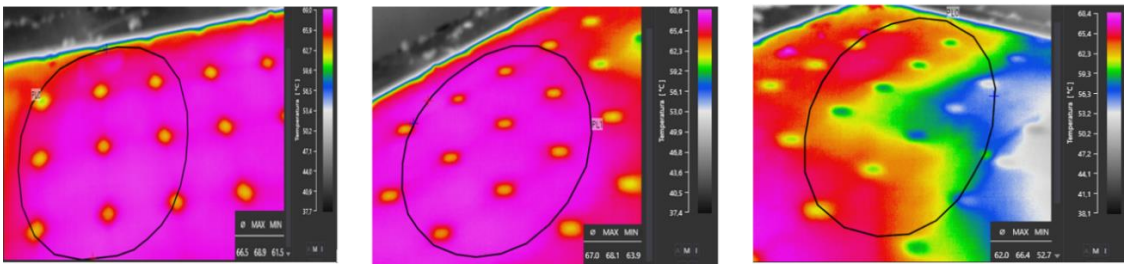

Z1 Z2 Z3

Figure10: Thermograms in Scenario 1.1 and Z1, Z2 and Z3.

The temperatures are not the same between the radiometer and the thermography, the difference being in most of the experiments around 5 ºC, because the sensor is not calibrated. The results show that accuracy is not critical for pattern recognition to detect dust on the PV panels. The sensor has not been calibrated intentionally because the main objective is to apply pattern recognition. Therefore, it is not necessary to know the real temperature on the PV panel. The calibration error is a systematic error applied in each measurement, i.e. the value of variation is almost constant in all cases [77].

Table 3: Temperatures with Radiometer sensor and thermographic camera in Scenario 1.1 Z1, Z2 and Z3

| | SI-111 (ºC) | WIRIS 640 (ºC) | Variation T (ºC) | Relative variation (%) |
|---|---|---|---|---|
| **Z1** | 60.9 | 66.5 | -5.59 | -8.4 |
| **Z2** | 61.0 | 67.0 | -5.96 | -8.8 |
| **Z3** | 56.6 | 62.0 | -5.35 | -8.6 |

Figure 11 shows the body and target temperatures given by the radiometric sensor for Scenario 1.1 over the time period and Z1, Z2 and Z3. It can be observed that the target temperature decreases in Z3, and in Z1 and Z2 are similar, being almost constant in each zone over the time period. The body temperature does not vary in each zone and over the time period.

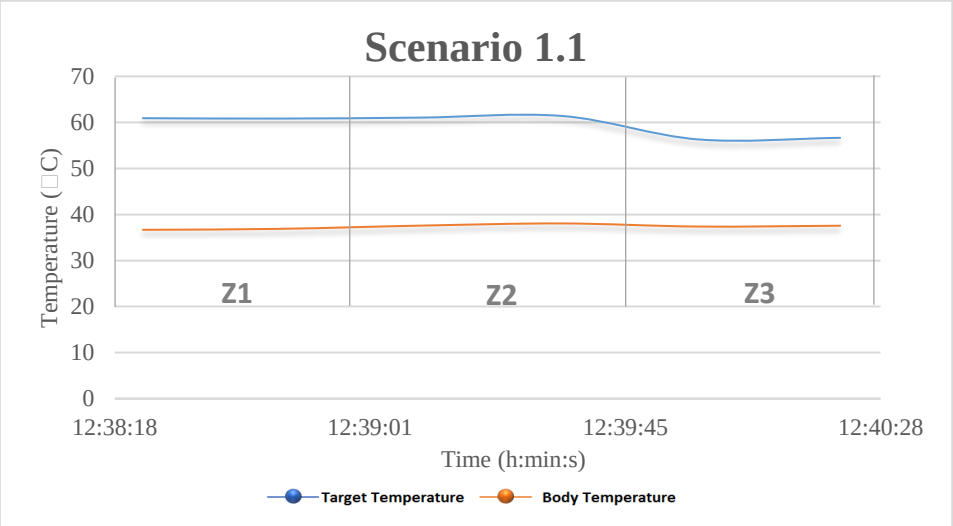


Figure 11. Target and body Temperatures given by the radiometric sensor for Scenario 1.1 over time periods and Z1, Z2 and Z3

Figure 12 indicates the thermographic results for Scenario 1.2, where the panel is set with an inclination of 70º regarding the vertical, and $\theta$ = 10º. Table 4 shows the temperatures given by the radiometer sensor Z1, Z2 and Z3. The results are similar to the results found in Scenario 1.1, where Z1 and Z2 show the same temperature by the radiometer sensor, and for Z3 a lower temperature is observed. These temperatures are higher that the temperatures found in Scenario 1.1. The same results are found in the thermography analysis. The differences are in the temperatures between the radiometer and thermography analysis in Scenario 1.2 and lower in Scenario 1.1. However, the relative variation is almost constant, but is a little less for Z3.

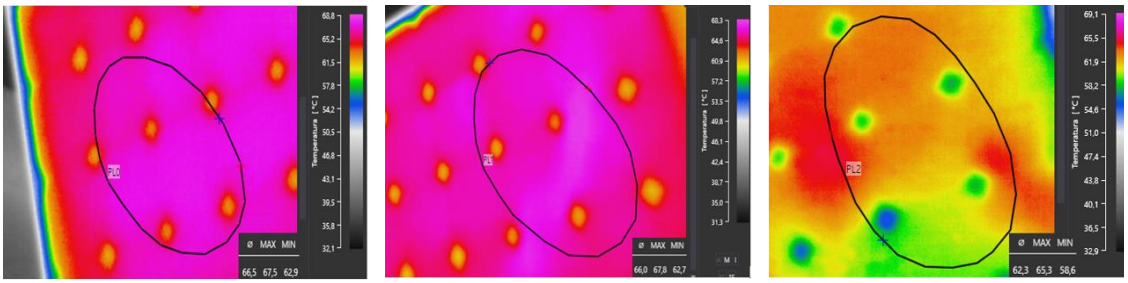

Z1 Z2 Z3

Figure 12: Thermograms in Scenario 1.3 and Z1, Z2 and Z3.

Table 4: Temperatures with Radiometer sensor and thermographic camera in Scenario 1.2 and Z1, Z2 and Z3

| | SI-111 (ºC) | WIRIS 640 (ºC) | Variation T (ºC) | Relative variation (%) |
|---|---|---|---|---|
| **Z1** | 61.1 | 66.5 | -5.4 | -8.8 |
| **Z2** | 61.0 | 66.0 | -4.9 | -8.1 |
| **Z3** | 58.2 | 62.3 | -4.0 | -6.9 |

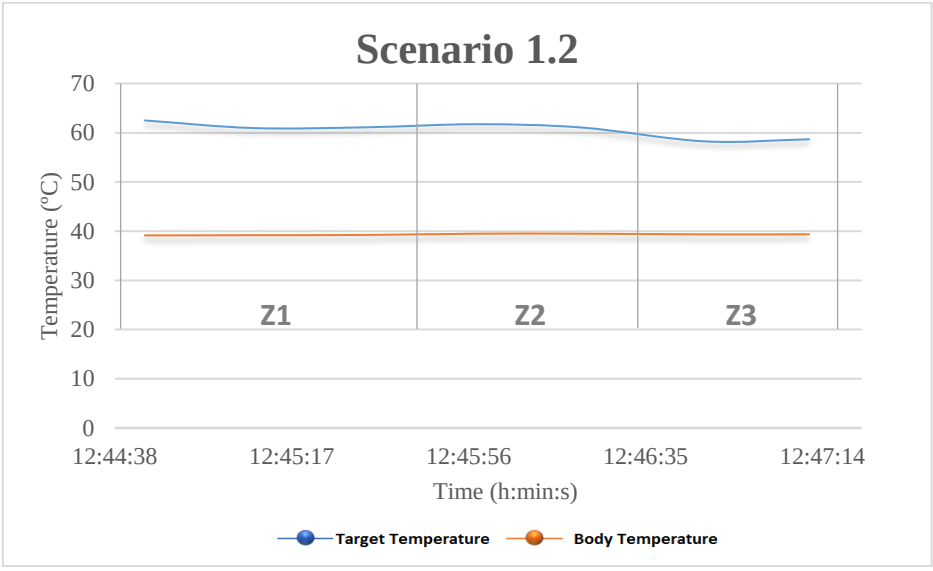


Figure 13. Target and body Temperatures given by the radiometric sensor for Scenario 1.2 over time periods and Z1, Z2 and Z3

Figure 14 and Table 5 shows the camera and sensor results for Scenario 1.3. The panel is set to 10º regarding to the vertical, and $\theta = 10º$. This scenario considers 4 zones because the dust area is higher than in Scenarios 1.1 and 1.3. Z1 and Z2 show higher temperatures in the measurements given by the thermography and radiometer analysis due to the fact that there is no dust. Z2 shows lower temperatures in both analyses because the border

indicates dust. The temperature is lower in Z3, where 25% of the area has dust, and a lower temperature is found in Z4, where the area studied is full of dust.

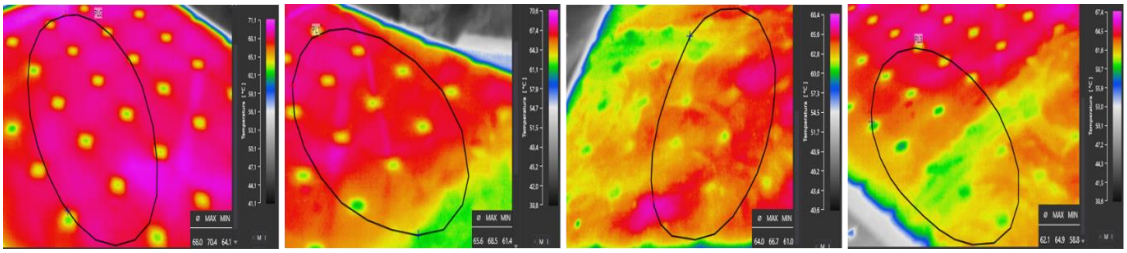

Z1 Z2 Z3 Z4

Figure 14: Thermograms in Scenario 1.3 and Z1, Z2, Z3 and Z4.

Table 5: Temperatures with Radiometer sensor and thermographic camera in Scenario 1.3 and Z1, Z2, Z3 and Z4

| | SI-111 (ºC) | WIRIS 640 (ºC) | Variation T (ºC) | Relative variation (%) |
|---|---|---|---|---|
| **Z1** | 61.8 | 68.0 | -6.2 | -9.1 |
| **Z2** | 59.8 | 65.6 | -5.8 | -8.8 |
| **Z3** | 58.1 | 64.0 | -5.9 | -9.2 |
| **Z4** | 56.1 | 62.1 | -6.0 | -9.7 |

Figure 15 shows the body and target temperatures given by the radiometric sensor for Scenario 1.3 over the time periods and Z1, Z2, Z3 and Z4. The target temperature decreases in Z3 and Z4. The temperatures in Z1 and Z2 are similar, but the temperature is a bit lower in Z2. The same result is shown in the thermography analysis. It is due to a real variation in the temperature on the PV panels, which is almost constant in each zone over the time period. The body temperature variation over the time period does not vary in each zone.

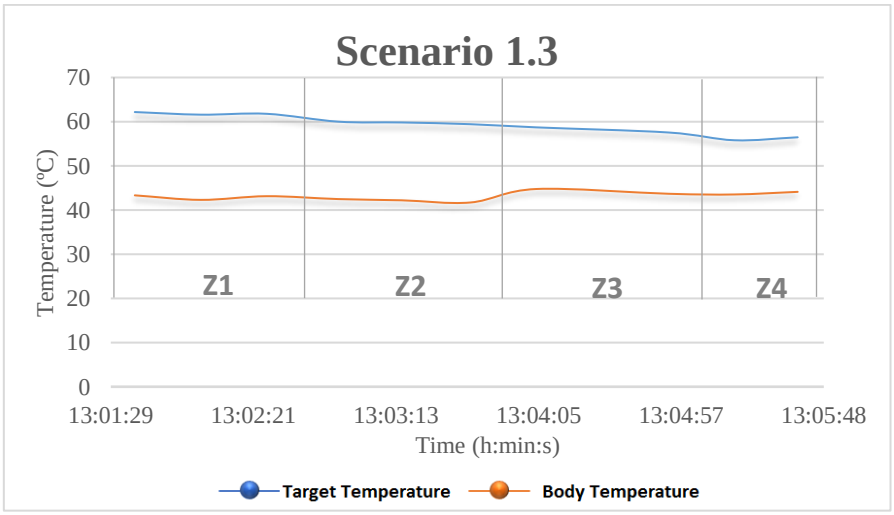


Figure 15. Target and body Temperatures given by the radiometric sensor for Scenario 1.3 over the time period and Z1, Z2 and Z3

The results in Z1 in each scenario are almost the same, and the same in Z2 in Scenarios 1.1 and 1.2. It shows that the measurements given by the radiometer and thermography analysis are the same considering different inclinations of the sensors and the panel. The temperatures found in Z3 in Scenarios 1.1 and 1.2 are lower than in Z1 and Z2, but they differ by 2ºC with the radiometer sensor. The same conclusions are reached in the thermographic analysis. It is observed that the temperature analysis obtained by the radiometer sensor in Z4 of Scenario 1.3 is lower than in Z3 in Scenarios 1.1 and 1.2, because the area with dust is greater, and the same conclusion is reached when a thermography analysis is tested.

The thermography analysis demonstrated coherence and uniformity in the measurements. The measurement accuracy is determined by the average relative variation in each experiment. Scenario 1.2 provides the highest degree of accuracy, the worst being in Scenario 1.3. The accuracy in this case depends clearly on the orientation of the radiometer sensor regarding the panel.

The experiments in all scenarios show that the radiometer sensor can detect dust on the panel surface, considering different positions of the panel and the sensor, and areas with of dust. The results found are also validated by the thermographic analysis.

**Validation of the results with the sensor embedded in the drone and the sensor calibrated/non-calibrated**

The results provided by the radiometric sensor not calibrated have been validated by the calibrated sensor and embedded in an AUV in the laboratory. The calibrated sensor provides the same results as those with the thermographic camera. The weather conditions were modified since the temperatures on the surfaces are lower. Table 6 shows the results with the panel at 70º regarding the vertical, being $\theta = 0º$ and 60º. A stable correlation is shown between the dataset.

Table 6. Radiometer senor calibrated and not calibrated embedded in a UAV, with $\theta = 0º$ and 60º.

| **EXPERIMENT AT 0º** | | **EXPERIMENT AT 60º** | |
|---|---|---|---|
| **Not Calibrated** | **Calibrated** | **Not Calibrated** | **Calibrated** |
| 21.82 | 24.16 | 22.13 | 24.19 |
| 18.39 | 20.59 | 17.90 | 20.05 |

Figures 16-18 show the temperatures of the sensor not calibrated considering different weather conditions. The weather conditions have been set according to the illuminance, measuring luminous flux per unit area on the PV surface. It was measured by the MT-912 light meter, with measures luminosity from 0 to 200000 Lux, with high accuracy of ±3% rdg ± 8 dgts (10000 Lux). The experiments were also done with the sensor calibrated, and the conclusions where the same to the results found previously. Therefore, only the measures given by the sensor not calibrated are showed in order to clarify the analysis.

Figure 16 presents temperatures for the scenarios with [59.6, 47, 23.2] klx and the surface clean. It shows that the temperature obtained rises when the illuminance increases.

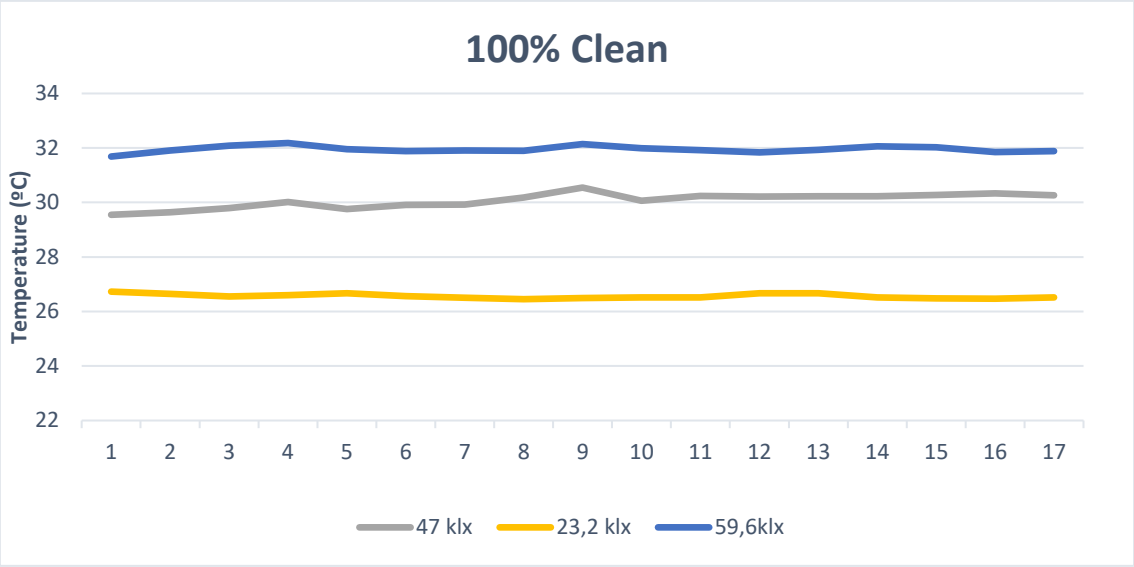


Figure 16. Temperatures with [59.6,47,23] klx and the surface clean

Figure 17 shows the temperatures with [59.6, 47, 23] klx and the surface is 100% dirty, i.e. the surface covered by dust. The temperatures for each illuminance are lowers that the temperatures given in Figure 17 due the dust on the PV surface. It also shows that the temperature increases regarding to the luminous flux per unit area (the same conclusion if the PV is clean, Figure 16).

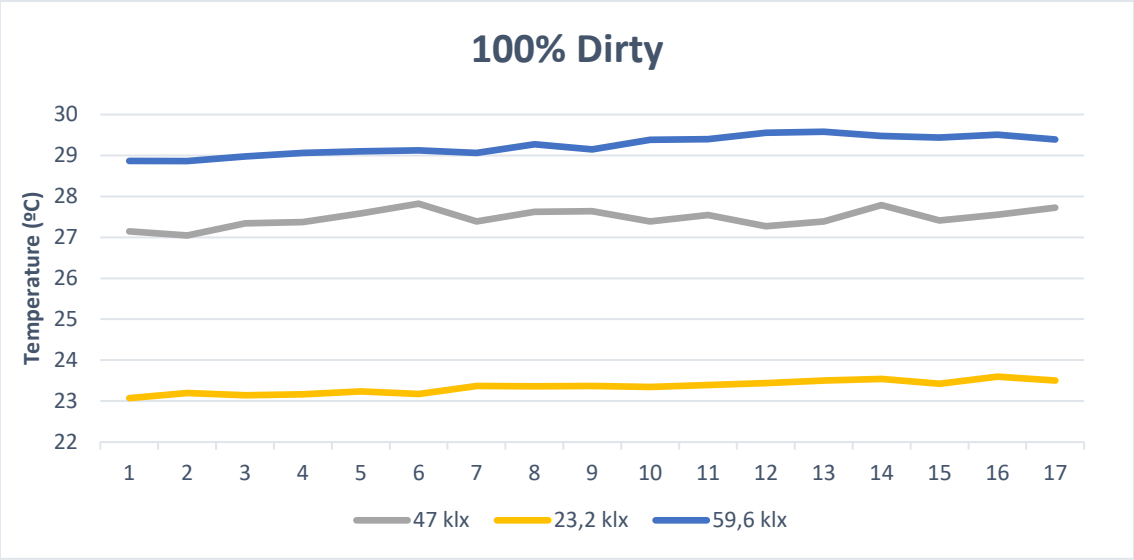


Figure 17. Temperatures with [59.6,47,23] klx and the surface dirty

Figure18 presents the temperatures obtained by the sensor not calibrated with [59.6,47,23] klx and the PV surface 50% dirty and 50% clean, higher than the temperatures when the PV surface is 100% dirty (Figure 17), but lower than the temperatures when the PV is clean (Figure 16). It validates the results obtained in the laboratory for these weather conditions. In every scenario considered, when the luminous emittance on the PV panel increases, the temperature measured rises.

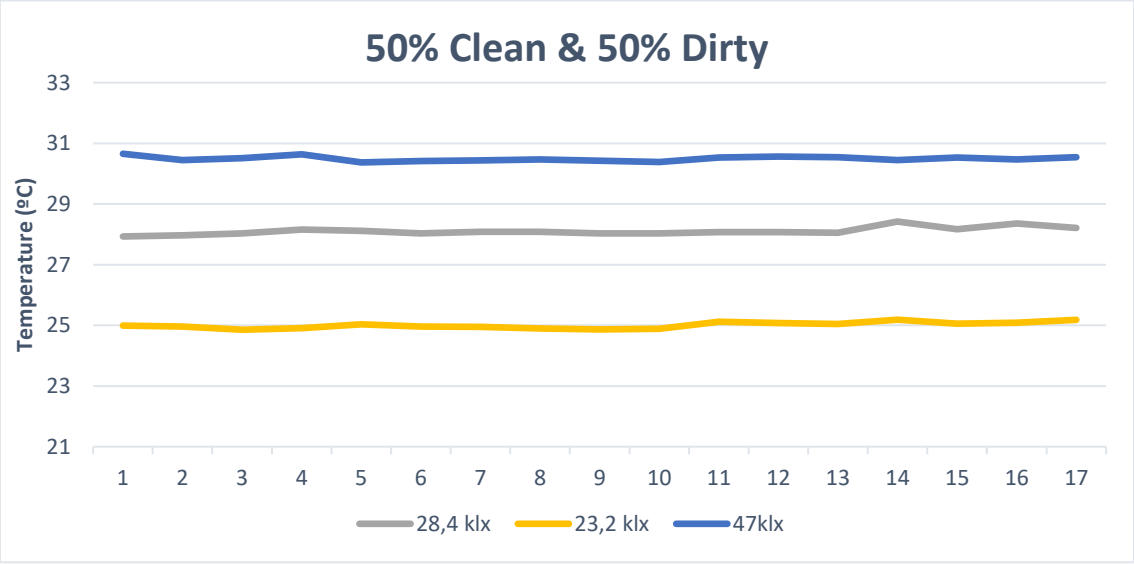


Figure 18. Temperatures with [59.6,47,23] klx and the surface 50% dirty and 50% clean.

# 5 Conclusions

This paper presents a new CMS employing a radiometer sensor connected to an Arduino board and embedded in an unmanned aerial vehicle. The objective is to detect dust in PV panels. A thermographic camera is used to validate the results in all the scenarios.

Three scenarios were analysed in order to consider different positions between the radiometer sensor and the panel.

The temperatures given by the new system are lower than the real one due to the fact that the sensor is not calibrated. The main objective is to detect and identify the surface condition of the panels by pattern recognition, i.e. if the surface indicates dust or not.

The results in cases where the area of the panel is free of dust in every scenario are almost the same. The temperatures decrease when the surfaces indicate dust, being the same conclusion in every scenario. The temperature also decreases when the area with dust is greater.

The results were validated for each experiment with the thermographic analysis, and the same conclusions were reached. Finally, the sensor not calibrated is analysed together with a calibrated sensor, doing measurements with the sensor embedded in the unmanned automatic vehicle and with different weather conditions.


# Acknowledgements

The work reported herewith has been financially supported by the Spanish Ministerio de Economía y Competitividad, under the Research Grant RTC-2016-5694-3.


# References


1. Panwar, N.; Kaushik, S.; Kothari, S. Role of renewable energy sources in environmental protection: A review. *Renewable and Sustainable Energy Reviews* **2011**, *15*, 1513-1524.
2. Solangi, K.; Islam, M.; Saidur, R.; Rahim, N.; Fayaz, H. A review on global solar energy policy. *Renewable and sustainable energy reviews* **2011**, *15*, 2149-2163.
3. Waldau, A.J. Snapshot of photovoltaics march 2016. **2016**.
4. Masson, G.; Latour, M.; Rekinger, M.; Theologitis, I.-T.; Papoutsi, M. Global market outlook for photovoltaics 2013-2017. *European Photovoltaic Industry Association* **2013**, 12-32.
5. Pliego Marugán, A.; García Márquez, F.P.; Pinar Pérez, J.M. Optimal maintenance management of offshore wind farms. *Energies* **2016**, *9*, 46.

6. Pliego Marugán, A.; García Márquez, F.P.; Lev, B. Optimal decision-making via binary decision diagrams for investments under a risky environment. *International Journal of Production Research* **2017**, 1-16.
7. Marugán, A.P.; Márquez, F.P.G. In *Scada and artificial neural networks for maintenance management*, International Conference on Management Science and Engineering Management, 2017; Springer: pp 912-919.
8. Pliego, A.; Márquez, F.P.G. Big data and web intelligence: Improving the efficiency on decision making process via bdd. In *Big data: Concepts, methodologies, tools, and applications*, IGI Global: 2016; pp 229-246.
9. Alberto Pliego Marugán, F.P.G.M. In *Fault-tree dynamic analysis*, Proceedings of the Eleventh International Conference on Condition Monitoring and Machinery Failure Prevention Technologies CM 2014 and MFPT 2014 (Ref. 115) ISBN: 9781634395052, 2015; British Institute of Non-Destructive Testing ( BINDT ): pp 1-9.
10. Garc, F.P.; Pliego, A.; Trapero, J.R. In *A new ranking method approach for decision making in maintenance management*, Proceedings of the Seventh International Conference on Management Science and Engineering Management, 2014; Springer: pp 27-38.
11. Guozhen, H.; Changsong, C.; Shanxu, D. In *Solutions for scada system communication reliability in photovoltaic power plants*, Power Electronics and Motion Control Conference, 2009. IPEMC'09. IEEE 6th International, 2009; IEEE: pp 2482-2485.
12. Tina, G.M.; Grasso, A.D. Remote monitoring system for stand-alone photovoltaic power plants: The case study of a pv-powered outdoor refrigerator. *Energy Conversion and Management* **2014**, *78*, 862-871.
13. Triki-Lahiani, A.; Bennani-Ben Abdelghani, A.; Slama-Belkhodja, I. Fault detection and monitoring systems for photovoltaic installations: A review. *Renewable and Sustainable Energy Reviews* **2018**, *82*, 2680-2692.
14. Hamdaoui, M.; Rabhi, A.; El Hajjaji, A.; Rahmoun, M.; Azizi, M. In *Monitoring and control of the performances for photovoltaic systems*, International Renewable Energy Congress, 2009.
15. Jiang, L.L.; Maskell, D.L. In *Automatic fault detection and diagnosis for photovoltaic systems using combined artificial neural network and analytical based methods*, Neural Networks (IJCNN), 2015 International Joint Conference on, 2015; IEEE: pp 1-8.
16. Karatepe, E.; Hiyama, T. In *Controlling of artificial neural network for fault diagnosis of photovoltaic array*, Intelligent System Application to Power Systems (ISAP), 2011 16th International Conference on, 2011; IEEE: pp 1-6.
17. Jaffery, Z.A.; Dubey, A.K.; Irshad; Haque, A. Scheme for predictive fault diagnosis in photo-voltaic modules using thermal imaging. *Infrared Physics & Technology* **2017**, *83*, 182-187.
18. Spataru, S.; Sera, D.; Kerekes, T.; Teodorescu, R. In *Photovoltaic array condition monitoring based on online regression of performance model*, Photovoltaic Specialists Conference (PVSC), 2013 IEEE 39th, 2013; IEEE: pp 0815-0820.
19. Touati, F.; Al-Hitmi, M.A.; Chowdhury, N.A.; Hamad, J.A.; San Pedro Gonzales, A.J.R. Investigation of solar pv performance under doha weather using a customized measurement and monitoring system. *Renewable Energy* **2016**, *89*, 564-577.
20. Dhimish, M.; Holmes, V.; Mehrdadi, B.; Dales, M. Diagnostic method for photovoltaic systems based on six layer detection algorithm. *Electric Power Systems Research* **2017**, *151*, 26-39.
21. Harrou, F.; Sun, Y.; Taghezouit, B.; Saidi, A.; Hamlati, M.-E. Reliable fault detection and diagnosis of photovoltaic systems based on statistical monitoring approaches. *Renewable Energy* **2018**, *116*, 22-37.
22. Garoudja, E.; Harrou, F.; Sun, Y.; Kara, K.; Chouder, A.; Silvestre, S. Statistical fault detection in photovoltaic systems. *Solar Energy* **2017**, *150*, 485-499.

23. Muñoz, C.Q.G.; Marquez, F.P.G.; Lev, B.; Arcos, A. New pipe notch detection and location method for short distances employing ultrasonic guided waves. *Acta Acustica united with Acustica* **2017**, *103*, 772-781.
24. Gómez Muñoz, C.Q.; García Márquez, F.P. A new fault location approach for acoustic emission techniques in wind turbines. *Energies* **2016**, *9*, 40.
25. Gallardo-Saavedra, S.; Hernández-Callejo, L.; Duque-Perez, O. Image resolution influence in aerial thermographic inspections of photovoltaic plants. *IEEE Transactions on Industrial Informatics* **2018**, *14*, 5678-5686.
26. Quater, P.B.; Grimaccia, F.; Leva, S.; Mussetta, M.; Aghaei, M. Light unmanned aerial vehicles (uavs) for cooperative inspection of pv plants. *IEEE Journal of Photovoltaics* **2014**, *4*, 1107-1113.
27. Gallardo-Saavedra, S.; Hernández-Callejo, L.; Duque-Perez, O. Technological review of the instrumentation used in aerial thermographic inspection of photovoltaic plants. *Renewable and Sustainable Energy Reviews* **2018**, *93*, 566-579.
28. Jiménez, A.A.; Muñoz, C.Q.G.; Marquez, F.P.G.; Zhang, L. In *Artificial intelligence for concentrated solar plant maintenance management*, Proceedings of the Tenth International Conference on Management Science and Engineering Management, 2017; Springer: pp 125-134.
29. Muñoz, C.Q.G.; Marquez, F.P.G.; Liang, C.; Maria, K.; Abbas, M.; Mayorkinos, P. In *A new condition monitoring approach for maintenance management in concentrate solar plants*, Proceedings of the ninth international conference on management science and engineering management, 2015; Springer: pp 999-1008.
30. Papaelias, M.; Cheng, L.; Kogia, M.; Mohimi, A.; Kappatos, V.; Selcuk, C.; Constantinou, L.; Muñoz, C.Q.G.; Marquez, F.P.G.; Gan, T.-H. Inspection and structural health monitoring techniques for concentrated solar power plants. *Renewable Energy* **2016**, *85*, 1178-1191.
31. Marugán, A.P.; Márquez, F.P.G.; Perez, J.M.P.; Ruiz-Hernández, D. A survey of artificial neural network in wind energy systems. *Applied Energy* **2018**, *228*, 1822-1836.
32. Jiménez, A.A.; Márquez, F.P.G.; Moraleda, V.B.; Muñoz, C.Q.G. Linear and nonlinear features and machine learning for wind turbine blade ice detection and diagnosis. *Renewable Energy* **2019**, *132*, 1034-1048.
33. Jiménez, A.A.; Gómez, C.Q.; Márquez, F.P.G. Concentrated solar plants management: Big data and neural network. In *Renewable energies*, Springer: 2018; pp 63-81.
34. Papaelias, M.; Márquez, F.P.G.; Ramirez, I.S. Concentrated solar power: Present and future. In *Renewable energies*, Springer: 2018; pp 51-61.
35. Breitenstein, O.; Warta, W.; Langenkamp, M. *Lock-in thermography: Basics and use for evaluating electronic devices and materials*. Springer Science & Business Media: 2010; Vol. 10.
36. Vermesan, O.; Friess, P.; Guillemin, P.; Gusmeroli, S.; Sundmaeker, H.; Bassi, A.; Jubert, I.S.; Mazura, M.; Harrison, M.; Eisenhauer, M. Internet of things strategic research roadmap. *Internet of Things-Global Technological and Societal Trends* **2011**, *1*, 9-52.
37. García Márquez, F.P.; Muñoz, G.; Quiterio, C.; Trapero Arenas, J.R. Structural health monitoring for concentrated solar plants. **2014**.
38. Molenbroek, E.; Waddington, D.; Emery, K. In *Hot spot susceptibility and testing of pv modules*, Photovoltaic Specialists Conference, 1991., Conference Record of the Twenty Second IEEE, 1991; IEEE: pp 547-552.
39. Muñoz, J.; Lorenzo, E.; Martínez‐Moreno, F.; Marroyo, L.; García, M. An investigation into hot‐spots in two large grid‐connected pv plants. *Progress in Photovoltaics: Research and applications* **2008**, *16*, 693-701.
40. Herraiz, Á.H.; Marugán, A.P.; Márquez, F.P.G. In *Optimal productivity in solar power plants based on machine learning and engineering management*, International

Conference on Management Science and Engineering Management, 2018; Springer: pp 983-994.
41. Barrientos, A.; Del Cerro, J.; Gutiérrez, P.; San Martín, R.; Martínez, A.; Rossi, C. Vehículos aéreos no tripulados para uso civil. Tecnología y aplicaciones. *Universidad politécnica de Madrid, Madrid* **2007**.
42. Ramirez, I.S.; Muñoz, C.Q.G.; Marquez, F.P.G. In *A condition monitoring system for blades of wind turbine maintenance management*, Proceedings of the tenth international conference on management science and engineering management, 2017; Springer: pp 3-11.
43. Muntwyler, U.; Schuepbach, E.; Lanz, M. In *Infrared (ir) drone for quick and cheap pv inspection*, Proceedings of the 31st European Photovoltaic Solar Energy Conference and Exhibition, 2015; pp 1804-1806.
44. Ramírez, I.S.; Marugán, A.P.; Márquez, F.P.G. In *Remotely piloted aircraft system and engineering management: A real case study*, International Conference on Management Science and Engineering Management, 2018; Springer: pp 1173-1185.
45. Pajares, G. Overview and current status of remote sensing applications based on unmanned aerial vehicles (uavs). *Photogrammetric Engineering & Remote Sensing* **2015**, *81*, 281-329.
46. Zorrilla-Casanova, J.; Philiougine, M.; Carretero, J.; Bernaola, P.; Carpena, P.; Mora-López, L.; Sidrach-de-Cardona, M. In *Analysis of dust losses in photovoltaic modules*, World Renewable Energy Congress-Sweden; 8-13 May; 2011; LinkÃ¶ ping; Sweden, 2011; Linköping University Electronic Press: pp 2985-2992.
47. Piliougine, M.; Carretero, J.; Sidrach-de-Cardona, M.; Montiel, D.; Sánchez-Friera, P. In *Comparative analysis of the dust losses in photovoltaic modules with different cover glasses*, Proceedings of 23rd European Solar Energy Conference, 2008; p 2698e2700.
48. García, M.; Marroyo, L.; Lorenzo, E.; Pérez, M. Soiling and other optical losses in solar-tracking pv plants in navarra. *Progress in Photovoltaics: Research and Applications* **2011**, *19*, 211-217.
49. Kimber, A.; Mitchell, L.; Nogradi, S.; Wenger, H. In *The effect of soiling on large grid-connected photovoltaic systems in california and the southwest region of the united states*, 2006 IEEE 4th World Conference on Photovoltaic Energy Conference, May 2006, 2006; pp 2391-2395.
50. Caron, J.R.; Littmann, B. Direct monitoring of energy lost due to soiling on first solar modules in california. *IEEE Journal of Photovoltaics* **2013**, *3*, 336-340.
51. Gostein, M.; Caron, J.R.; Littmann, B. In *Measuring soiling losses at utility-scale pv power plants*, 2014 IEEE 40th Photovoltaic Specialist Conference (PVSC), 8-13 June 2014, 2014; pp 0885-0890.
52. Pedersen, H.; Strauss, J.; Selj, J. Effect of soiling on photovoltaic modules in norway. *Energy Procedia* **2016**, *92*, 585-589.
53. Javed, W.; Wubulikasimu, Y.; Figgis, B.; Guo, B. Characterization of dust accumulated on photovoltaic panels in doha, qatar. *Solar Energy* **2017**, *142*, 123-135.
54. Burton, P.D.; King, B.H. Application and characterization of an artificial grime for photovoltaic soiling studies. *IEEE Journal of Photovoltaics* **2014**, *4*, 299-303.
55. Acciani, G.; Simione, G.; Vergura, S. In *Thermographic analysis of photovoltaic panels*, International Conference on Renewable Energies and Power Quality (ICREPQ'10), Granada, Spain, March, 2010; pp 23-25.
56. Jamil, W.J.; Abdul Rahman, H.; Shaari, S.; Salam, Z. Performance degradation of photovoltaic power system: Review on mitigation methods. *Renewable and Sustainable Energy Reviews* **2017**, *67*, 876-891.
57. Mazumder, M.K.; Horenstein, M.N.; Heiling, C.; Stark, J.W.; Sayyah, A.; Yellowhair, J.; Raychowdhury, A. In *Environmental degradation of the optical surface of pv modules and solar mirrors by soiling and high rh and mitigation methods for minimizing energy*

*yield losses*, Photovoltaic Specialist Conference (PVSC), 2015 IEEE 42nd, 2015; IEEE: pp 1-6.
58. Moharram, K.A.; Abd-Elhady, M.S.; Kandil, H.A.; El-Sherif, H. Influence of cleaning using water and surfactants on the performance of photovoltaic panels. *Energy Conversion and Management* **2013**, *68*, 266-272.
59. Aly, S.P.; Gandhidasan, P.; Barth, N.; Ahzi, S. In *Novel dry cleaning machine for photovoltaic and solar panels*, Renewable and Sustainable Energy Conference (IRSEC), 2015 3rd International, 2015; IEEE: pp 1-6.
60. Tucci, M.; Salurso, E.; Roca, F.; Palma, F. Dry cleaning process of crystalline silicon surface in a・si: H/c・si heterojunction for photovoltaic applications. *Thin Solid Films* **2002**, *403*, 307-311.
61. Kaushika, N.D.; Gautam, N.K. Energy yield simulations of interconnected solar pv arrays. **2003**.
62. Chamberlin, C.E.; Lehman, P.; Zoellick, J.; Pauletto, G. Effects of mismatch losses in photovoltaic arrays. *Solar energy* **1995**, *54*, 165-171.
63. Petrone, G.; Spagnuolo, G.; Vitelli, M. Analytical model of mismatched photovoltaic fields by means of lambert w-function. *Solar energy materials and solar cells* **2007**, *91*, 1652-1657.
64. Chouder, A.; Silvestre, S. Analysis model of mismatch power losses in pv systems. *Journal of Solar Energy Engineering* **2009**, *131*, 024504.
65. Palmer, J.M.; Grant, B.G. *The art of radiometry*. SPIE Press Bellingham, WA, USA: 2010.
66. Muñoz, C.Q.G.; Márquez, F.P.G.; Tomás, J.M.S. Ice detection using thermal infrared radiometry on wind turbine blades. *Measurement* **2016**, *93*, 157-163.
67. Usamentiaga, R.; Venegas, P.; Guerediaga, J.; Vega, L.; Molleda, J.; Bulnes, F. Infrared thermography for temperature measurement and non-destructive testing. *Sensors* **2014**, *14*, 12305-12348.
68. Ibarra-Castanedo, C.; Genest, M.; Piau, J.-M.; Guibert, S.; Bendada, A.; Maldague, X.P. Active infrared thermography techniques for the nondestructive testing of materials. *Ultrasonic and advanced methods for nondestructive testing and material characterization* **2007**, 325-348.
69. Coutts, A.M.; Harris, R.J.; Phan, T.; Livesley, S.J.; Williams, N.S.; Tapper, N.J. Thermal infrared remote sensing of urban heat: Hotspots, vegetation, and an assessment of techniques for use in urban planning. *Remote Sensing of Environment* **2016**, *186*, 637-651.
70. Navabi, R.; Abedi, S.; Hosseinian, S.H.; Pal, R. On the fast convergence modeling and accurate calculation of pv output energy for operation and planning studies. *Energy Conversion and Management* **2015**, *89*, 497-506.
71. Gwandu, B.; Creasey, D. Humidity: A factor in the appropriate positioning of a photovoltaic power station. *Renewable Energy* **1995**, *6*, 313-316.
72. Mekhilef, S.; Saidur, R.; Kamalisarvestani, M. Effect of dust, humidity and air velocity on efficiency of photovoltaic cells. *Renewable and Sustainable Energy Reviews* **2012**, *16*, 2920-2925.
73. Dubey, S.; Sarvaiya, J.N.; Seshadri, B. Temperature dependent photovoltaic (pv) efficiency and its effect on pv production in the world – a review. *Energy Procedia* **2013**, *33*, 311-321.
74. Skoplaki, E.; Palyvos, J.A. Operating temperature of photovoltaic modules: A survey of pertinent correlations. *Renewable energy* **2009**, *34*, 23-29.
75. Hove, T. A method for predicting long-term average performance of photovoltaic systems. *Renewable Energy* **2000**, *21*, 207-229.
76. Skoplaki, E.; Palyvos, J.A. On the temperature dependence of photovoltaic module electrical performance: A review of efficiency/power correlations. *Solar Energy* **2009**, *83*, 614-624.

77. Minkina, W.; Dudzik, S. *Infrared thermography: Errors and uncertainties*. John Wiley & Sons: 2009.